Mutual neutralization in $H^+ + H^-$ collisions: An improved theoretical model

Johan Hörnquist,* Patrik Hedvall, and Åsa Larson
Department of Physics, Stockholm University, AlbaNova University Center, SE-106 91 Stockholm, Sweden

Ann E. Orel
Department of Chemical Engineering, University of California, Davis, California 95616, USA

(Received 10 August 2022; accepted 6 December 2022; published 22 December 2022)

The total and differential cross sections of mutual neutralization in $H^+ + H^-$ collisions are calculated *ab initio* and fully quantum mechanically for energies between 0.001 and 600 eV. Effects which have not previously been considered in studies on mutual neutralization (MN) for this system, such as inclusion of rotational couplings and autoionization, are investigated. Adiabatic potential curves corresponding to the relevant states of $^1\Sigma_g^+$, $^1\Sigma_u^+$, $^1\Pi_g$ and $^1\Pi_u$ symmetries as well as radial and rotational nonadiabatic couplings are computed *ab initio*. A quasidiabatic model is developed and applied in order to investigate the importance of higher excited states as well as the inclusion of autoionization. Molecular data for the lowest electronic resonant state in each symmetry are obtained by performing electron scattering calculations. It is shown that rotational couplings cause a significant increase of the total MN cross section while autoionization plays a minor role as a loss mechanism. Additionally, a differential cross section is obtained that is symmetric around $\theta = 90^\circ$. This result is in disagreement with a previous theoretical calculation where it was found that the differential cross section is dominated by backwards scattering.

DOI: 10.1103/PhysRevA.106.062821

I. INTRODUCTION

The process

$$H^+ + H^- \rightarrow H(1s) + H(n), \tag{1}$$

where n is the principal quantum number, is the most basic example of mutual neutralization (MN) and has therefore attracted much attention over the years. The relative simplicity of the system makes it optimal to test out theoretical models in order to build a deeper understanding of the process, which could then serve as a starting point to study more complex systems. Recently, there has been a renewed interest in MN between atomic ions at the DESIREE facility in Stockholm and at Louvain-la-Neuve in Belgium, and measurements have been performed on MN in collisions of $Li^+ + D^-$ [1], $Na^+ + D^-$ [2], $Mg^+ + D^-$ [3], and $O^+/N^+ + O^-$ [4].

Early measurements on the $H^+ + H^-$ MN cross section [5–8] were in mutual agreement with each other and the cross section showed well defined structures. Despite the relative simplicity of the system, none of the theoretical calculations around that time [9–16] could reproduce the structures nor the overall magnitude of the cross section. Later measurements made by Szucs *et al.* [17] yielded a cross section that differs significantly from the earlier measurements and show no such structures. Peart *et al.* [18] subsequently remeasured the cross section and the result was found to agree with the new measurement of Szucs *et al. Ab initio* semiclassical calculations using a one-electron close coupling model by Sidis *et al.* [16] supported the newer measurements. Additionally, Fussen and Kubach [19] did a quantum mechanical calculation using a one-electron close-coupling model and obtained a cross section that agrees with the low-energy data of [17] and match the theoretical result of [16] within 10%. A later refined experiment by Peart *et al.* [20] lends further support to the result of Szucs *et al.*, and these measurements are now considered to be correct. For collision energies $\leqslant 10$ eV, Eerden *et al.* [21] used a multistate Landau-Zener (LZ) model and their result agrees with that of Fussen and Kubach within 20%.

In more recent times, some of the present authors made *ab initio* fully quantum mechanical studies of $H^+ + H^-$ MN [22,23] in which the total cross section was found to be in good agreement with experiment [17,18,20] for energies between 10 and 100 eV. It was also found to be in good agreement with the calculation by Eerden *et al.* and about a factor of 1.2 larger than the calculation by Fussen and Kubach. In the *ab initio* calculations, excited states were included of $^1\Sigma_g^+$ and $^1\Sigma_u^+$ symmetries up to the asymptotic limit $H(1s) + H(n = 3)$. It is generally thought that states associated with $n \geqslant 4$ have a small contribution to the total cross section based on the fact that these states only have nonadiabatic couplings at small internuclear distances. An exception are the $n = 4$ states which have avoided crossings with the ionic state at very large internuclear distances

*johan.hornquist@fysik.su.se

Published by the American Physical Society under the terms of the Creative Commons Attribution 4.0 International license. Further distribution of this work must maintain attribution to the author(s) and the published article's title, journal citation, and DOI. Funded by Bibsam.

($R \approx 280\,a_0$). These are, however, expected to be insignificant [9,14,16]. The MN branching ratios to $H(1s) + H(n)$ for different n have also been measured experimentally using an ion-ion single-pass merged beam apparatus [23]. Computing branching ratios is more difficult than computing the total cross section and is therefore a more stringent test of the theory. The *ab initio* calculations of [22,23] are in agreement with the measured branching ratios for energies up to 50 eV, but deviates for larger energies. Naturally, this raises the question whether higher excited states contribute. Another effect which has not previously been considered is the effect of rotational coupling which couples the $^1\Sigma^+_{g/u}$ states to $^1\Pi_{g/u}$ states. It has been pointed out by Bardsley [24], referring to unpublished calculations on $H^+ + H^-$ MN by Browne and Victor, that such couplings could be important for MN. This could potentially explain the difference between calculated and measured branching ratios at high collision energies.

The goal of present article is to return to the $H^+ + H^-$ collision system and investigate the limitations of the approximations by including effects that have not previously been included, such as excited states associated with the $n \geqslant 4$ limits, rotational couplings, and inclusion of autoionization from electronic resonant states. There are few systems that have been studied as much as the H_2 system. However, there is not yet any study that reports all adiabatic potential energy curves and radial and rotational couplings for the states in all symmetries we here consider. Therefore, we have here computed all the relevant adiabatic potential curves as well as radial and rotational nonadiabatic couplings *ab initio*. We have performed electron scattering calculations to obtain information of the electronic resonant states. While the *ab initio* potentials and couplings are used to describe the lower electronic states, a quasidiabatic model is developed to include both the lowest electronic resonant state in each symmetry as well as an arbitrary number of Rydberg states. The total and differential cross sections as well as branching ratios are computed for the $H^+ + H^-$ MN process. With this model, the importance of higher excited states can be studied as well as the role of autoionization from electronic resonant states. The same model can also be used to study other processes such as associative ionization, dissociative recombination, and ion-pair formation.

The article is structured as follows. In Sec. II we present our calculated adiabatic potentials curves, radial nonadiabatic couplings, and rotational couplings. In this section we also discuss the resonant states and electronic couplings. The inclusion of rotational couplings and the quasidiabatic model are described in Sec. III. Finally, the $H^+ + H^-$ MN differential and total cross sections as well as branching ratios are presented in Sec. IV. Throughout the article we use atomic units, unless otherwise specified.

II. POTENTIAL CURVES AND COUPLINGS

A. Potential curves

MN is a process driven by nonadiabatic couplings between ionic and covalent states and as such it involves several excited states. Thus, in order to obtain a reliable theoretical description of the process it is crucial to have accurate

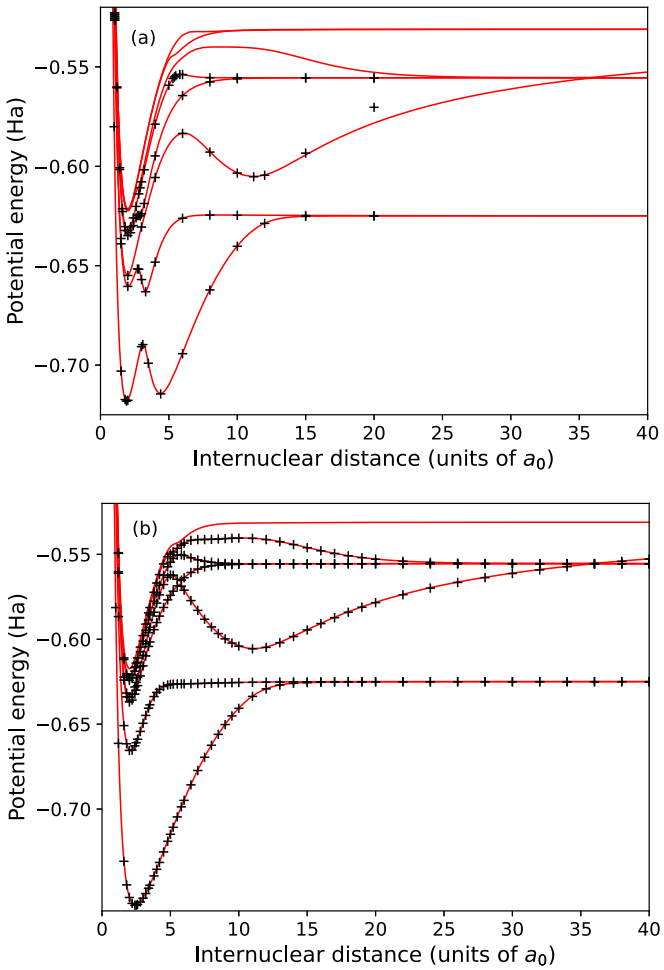

FIG. 1. Adiabatic potential energy curves (red solid lines) of electronic states in (a) $^1\Sigma^+_g$ symmetry in comparison to the potentials calculated by Wolniewicz and Dressler [25] (black crosses) and (b) of $^1\Sigma^+_u$ symmetry in comparison to the potentials calculated by Staszewska and Wolniewicz [26] (black crosses).

data on the relevant potential curves and nonadiabatic couplings. The adiabatic potential curves corresponding to the states (1–11) $^1\Sigma^+_g$, (1–10) $^1\Sigma^+_u$, (1–6)$^1\Pi_g$, and (1–6)$^1\Pi_u$ have been computed using the DALTON program [27,28]. These calculations were carried out using the full Configuration Interaction (CI) method with a hydrogen basis set composed of $(11s, 8p, 7d, 6f)$ primitive functions contracted to $(9s, 8p, 7d, 6f)$. This basis set was obtained by adding a set of $(5s, 5p, 5d, 5f)$ diffuse functions to the cc-pVQZ basis set [29]. The exponents of the diffuse functions are geometric series with ratios $k_s = 2.6$, $k_p = 2.6$, $k_d = 2.8$, and $k_f = 3.2$, starting from the most diffuse functions of the cc-pVQZ basis set. The exponents were optimized in order to accurately describe the $n = 4$ dissociation limit and the large distance avoided crossings as it is crucial to have an accurate description of these avoided crossings in order to compute reliable cross sections for the MN process.

Figure 1 shows the adiabatic potentials of the [Fig. 1(a)] (2–9) $^1\Sigma^+_g$ electronic states and the [Fig. 1(b)] (1–7) $^1\Sigma^+_u$ electronic states, for internuclear distances between 0 and $40\,a_0$. In both $^1\Sigma^+_g$ and $^1\Sigma^+_u$ symmetries there is one state that

asymptotically correlates with the ion-pair $H^+ + H^-$, while the other states correlate with covalent limits of $n = 2$–4. The $X\,^1\Sigma_g^+$ potential correlating with the $n = 1$ limit is not displayed in the figure. The potentials exhibit a large number of avoided crossings, both for large ($\sim 36\,a_0$), intermediate ($\sim 12\,a_0$), and small ($\sim 4\,a_0$) internuclear distances. At small internuclear distances, the potentials (2–3) $^1\Sigma_g^+$ have the characteristic double well, arising from the interaction with the lowest electronic resonant state of $^1\Sigma_g^+$ symmetry.

In order to assess the quality of the calculated potentials, they have been compared to previously calculated potentials. The most accurate data on the (2–6) $^1\Sigma_g^+$ potentials are from Wolniewicz and Dressler [25]. A comparison of the absolute energies with our potentials yields excellent agreement with differences varying in the order of 1×10^{-4} to 1×10^{-6} hartree. For the (1–6) $^1\Sigma_u^+$ we compare our data to that of Staszewska and Wolniewicz [26], for which we also find excellent agreement, with differences typically varying between 1×10^{-4} to 1×10^{-6} hartree. For the (1–2) $^1\Pi_g$ and (1–4) $^1\Pi_u$, the most accurate calculations are those by Wolniewicz [30] and Wolniewicz and Staszewska [31], respectively. A comparison, shown in Fig. 2, to our computed data yields excellent agreement, of the same order of magnitude as for the $^1\Sigma_g^+$ and $^1\Sigma_u^+$ potentials.

For the higher excited states (correlating with the $n = 4$ limit) we compare our results to that of Corongiu and Clementi [32,33]. They have systematically computed a variety of H_2 potentials, including (1–11) $^1\Sigma_g^+$ and (1–10) $^1\Sigma_u^+$. Our calculated potentials (7–9) $^1\Sigma_g^+$ are in good agreement with theirs with differences in absolute energies of the order of 1×10^{-4} to 1×10^{-5} hartree, our potentials being lower for some points of internuclear distance. The states (10–11) $^1\Sigma_g^+$ are in good agreement with their results for internuclear distances larger than 5 a_0. However, the agreement is less satisfactory below 5 a_0 where their potentials are much lower in energy. A similar analysis for the potentials of $^1\Sigma_u^+$ symmetry shows that the potentials (8–10) $^1\Sigma_u^+$ are too high in energy below 7 a_0. The $n = 4$ states relevant for our study have also been calculated by Nakashima and Nakatsuji [34] and Kurokawa *et al.* [35] who used their free-complement theory to compute potentials of, among others, the states (1–11) $^1\Sigma_g^+$, (1–6) $^1\Sigma_u^+$, (1–4) $^1\Pi_g$, and (1–4) $^1\Pi_u$. Here we also see excellent agreement with most of our data. The exception is again the states (10–11) $^1\Sigma_g^+$ and (8–10) $^1\Sigma_u^+$, which are much higher than their potentials below 5 and 7 a_0, respectively.

To further asses the accuracy of the calculated adiabatic potential curves at small internuclear distances, we have also computed the adiabatic effective quantum numbers from the calculated potentials,

$$\nu_i^{\rm ad}(R) = \frac{1}{\sqrt{2\left[V_{\rm ion}(R) - V_i^{\rm ad}(R)\right]}}. \qquad (2)$$

In Fig. 3 we show the effective quantum numbers obtained for states of $^1\Sigma_g^+$ symmetry in comparison those obtained from the potential curves of Corongiu and Clementi [32]. A similar comparison was made also to the other above mentioned references. From these comparisons, as is also evident in Fig. 3, we can draw the conclusion that we have not obtained a

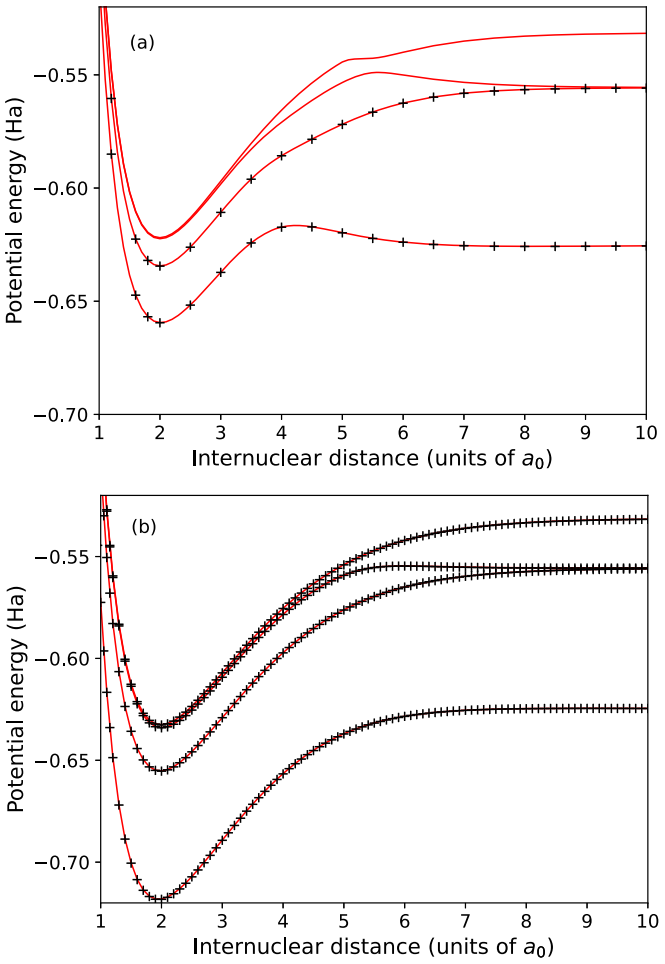

FIG. 2. Adiabatic potential energy curves (red solid lines) of electronic states in (a) $^1\Pi_g$ symmetry in comparison to the potentials calculated by Wolniewicz [30] (black crosses) and (b) of $^1\Pi_u$ symmetry in comparison to the potentials calculated by Wolniewicz and Staszewska [31] (black crosses).

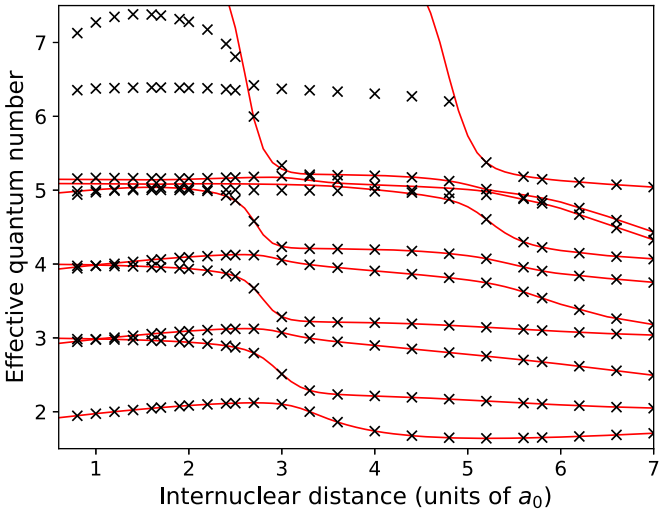

FIG. 3. Effective quantum numbers of electronic states in $^1\Sigma_g^+$ symmetry (red solid lines) in comparison those computed from the potentials curves of Corongiu and Clementi [32] (black crosses).

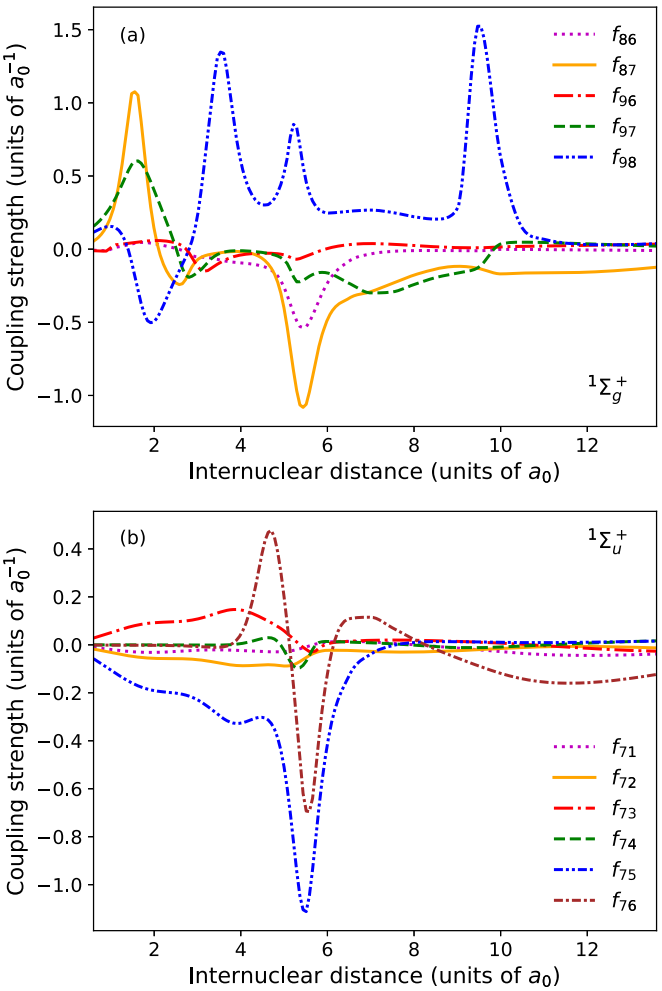

FIG. 4. Radial nonadiabatic coupling elements of electronic states in (a) $^1\Sigma_g^+$ symmetry and (b) $^1\Sigma_u^+$ symmetry. The notation f_{ij} denotes the radial coupling between states i and j.

satisfactory description at small internuclear distances of the highest excited calculated potentials ($10\,^1\Sigma_g^+$, $11\,^1\Sigma_g^+$, $8\,^1\Sigma_u^+$, $9\,^1\Sigma_u^+$, $10\,^1\Sigma_u^+$, $5\,^1\Pi_g$, $6\,^1\Pi_g$, $5\,^1\Pi_u$, and $6\,^1\Pi_u$). Given the above analysis we made the decision not to include the mentioned potentials in our calculations of the MN cross sections.

B. Radial and rotational couplings

The radial nonadiabatic couplings,

$$f_{ij}^{\Lambda} = \langle \Phi_{i\Lambda} | \frac{\partial}{\partial R} | \Phi_{j\Lambda} \rangle \,, \tag{3}$$

among all adiabatic states included in the model have been calculated using a three-point version of the finite difference method, as described in Ref. [36], with a derivative step length of $\Delta R = 5 \times 10^{-5}\ a_0$. This method allows for the convergence of the result with respect to the basis set and wave functions used. The couplings of Eq. (3) only couple states of the same parity and the label g/u is omitted for a cleaner notation. In Fig. 4 we show some of the important nonadiabatic coupling elements to the $n = 4$ states in the symmetries [Fig. 4(a)] $^1\Sigma_g^+$ and [Fig. 4(b)] $^1\Sigma_u^+$. These couplings have peaks at various internuclear distances below about 12 a_0 and are significant in size only in that region (we here consider internuclear distances $\leqslant 55\ a_0$). To our knowledge, the radial nonadiabatic couplings involving the $n = 4$ states in $^1\Sigma_g^+$ and $^1\Sigma_u^+$ symmetries have not been published before. Therefore no comparison has been made to the literature.

The couplings between the states (2–6) $^1\Sigma_g^+$ (not shown in Fig. 4) are in good agreement with the couplings calculated by Wolniewicz and Dressler [25] for internuclear distances up to 15 a_0. Some minor deviations can be found for larger internuclear distances. However, their calculations do not extend further than 20 a_0. Most of the nonadiabatic couplings among the states (1–6) $^1\Sigma_u^+$ and (1–4) $^1\Pi_u$ are in agreement with those calculated by Wolniewicz *et al.* [37]. Among the $^1\Sigma_u^+$ states, some disagreement is found primarily around the curve crossing at 36 a_0. For internuclear distances larger than 36 a_0, the $n = 3$ states are almost degenerate and beyond the curve crossing the order of the states in our calculation is switched compared to Ref. [37]. Consequently, the radial couplings of Ref. [37] that involve the $3\,^1\Sigma_u^+$ state become equal to our couplings that involve the $4\,^1\Sigma_u^+$ state and vice versa after the $R = 36\ a_0$ curve crossing. The couplings of $^1\Pi_u$ symmetry are in good agreement with [37] up to 10 a_0.

The rotational couplings between the $^1\Sigma_g^+$ and $^1\Pi_g$ states and between the $^1\Sigma_u^+$ and $^1\Pi_u$ states included in our model have also been calculated. Some of these couplings are shown in Fig. 5 in comparison to previously published results. For internuclear distances $<15\ a_0$, the calculated rotational couplings between the $^1\Sigma_u^+$ and $^1\Pi_u$ symmetries are in excellent agreement with Ref. [37], but some of the couplings disagree for larger distances. The adiabatic potential curves and radial and rotational nonadiabatic couplings are available as Supplemental Material [39].

C. Resonant states and electronic couplings

In order to include autoionization from electronic resonant states and to include Rydberg states, a quasidiabatic model (described in Sec. III B) was used. The model includes the complex resonant state potential, electronic couplings between the resonant state and the Rydberg series and the diabatic quantum defects. These quantities are needed both for internuclear distances when the resonant state lies in the continuum, i.e., above the ion potential, and also for internuclear distances where the resonant state lies in the discrete spectrum. We have performed electron scattering calculations using the Complex-Kohn variational method [40] to determine the potential as well as total and partial autoionization widths of the lowest resonant state in the $^1\Sigma_g^+$, $^1\Sigma_u^+$, $^1\Pi_g$, and $^1\Pi_u$ symmetries, respectively. In these calculations a modified version of the basis set described in Sec. II A was used, where the most diffuse s, p, d, and f functions were eliminated leaving a basis set of $(5s, 6p, 5d, 1f)$. A full CI was used in this basis to obtain a set of nine natural orbitals, $3\sigma_g$, $2\sigma_u$, $1\pi_{ux}$, $1\pi_{uy}$, $1\pi_{gx}$, and $1\pi_{gy}$ which formed the active space for the scattering calculation. Full CI was carried out in the active space and all single external excitations were included out of the reference configurations. The electron scattering variational calculations included spherical harmonics up to $l = 6$. The calculations were carried out in each symmetry at a fixed internuclear distance. At the resonant energy E_r, the

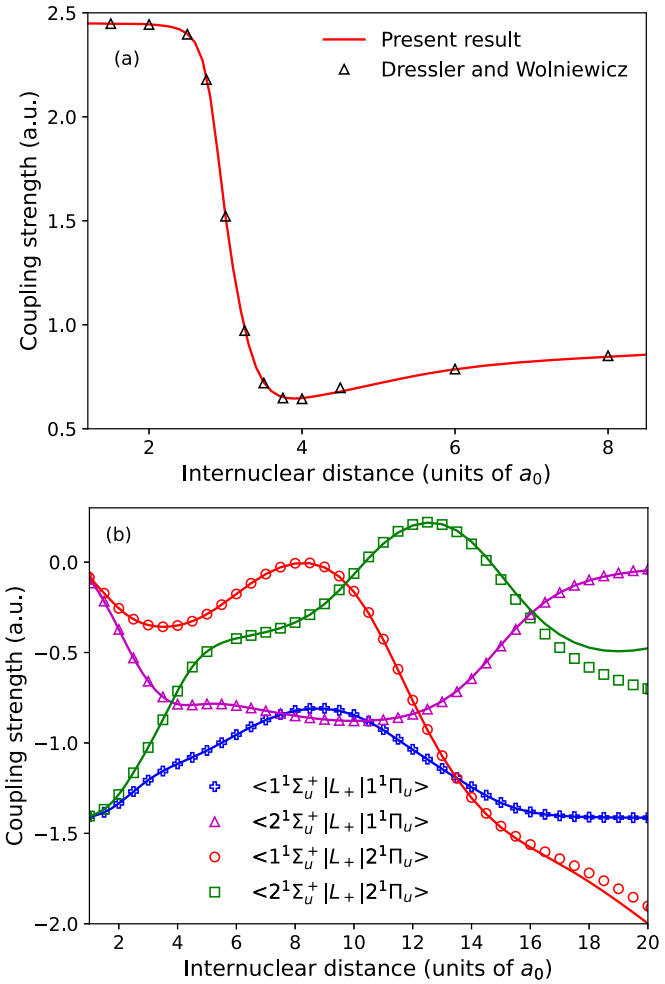

FIG. 5. Rotational couplings between (a) the states $3\,^1\Sigma_g^+$ and $1\,^1\Pi_g$ compared to the results of Dressler and Wolniewicz [38] and (b) between states of $^1\Sigma_u^+$ and $^1\Pi_u$ symmetries (solid lines) compared to the results of Wolniewicz *et al.* [37] (symbols).

electron can be temporarily captured into a "metastable state," which will cause a sharp variation of the elastic scattering cross section.

From the eigenphase sum $\Delta(E)$ of the S-matrix one can obtain the resonant state position relative to the ion, E_r, and the total autoionization width, Γ, by fitting it to a Breit-Wigner form [41]

$$\Delta(E) = \sum_n \delta_n(E) = \Delta_{bg}(E) + \arctan\left[\frac{\Gamma}{2(E_r - E)}\right]. \quad (4)$$

The partial widths can then be extracted by a fit of the S-matrix elements [42]

$$S_{ij}(E) = S_{ij}^{bg}(E) - i\frac{\gamma_i\gamma_j}{E - E_r + i\Gamma/2}, \quad (5)$$

where $\Gamma = \sum_i \Gamma_i = \sum_i |\gamma_i|^2$. From the background scattering matrix, S^{bg}, which is fitted to a second degree polynomial in energy, one can obtain the diabatic quantum defects.

For geometries where the potential of the resonant state has crossed the ion we have taken another approach where we perform an optimization procedure to obtain the relevant quantities. In this procedure, the resonant state energy, electronic couplings and diabatic quantum defects are parameterized by their values at sufficiently separated points of internuclear distance in the region where the interaction between the Rydberg states and resonant state takes place. A quasidiabatic potential matrix is then set up and diagonalized. The sum

$$f = \sum_{i,j} \left(V_j^{\rm ad}(R_i) - V_j^{\rm diag.}(R_i)\right)^2, \quad (6)$$

is then minimized using simulated annealing [43]. The subscript i refers to different R points, $V_j^{\rm ad}$ to the jth *ab initio* adiabatic potential energy curve and $V_j^{\rm diag.}$ denotes the jth eigenvalue of the quasidiabatic potential matrix. In order to cover the full range of internuclear distances we have combined the optimization procedure with the scattering calculations. We define an interaction region (2.0–4.0 a_0 for $^1\Sigma_g^+$, 4.0–6.0 a_0 for $^1\Sigma_u^+$, and 3.0–6.0 a_0 for $^1\Pi_g$ and $^1\Pi_u$), which approximately spans the region of the avoided crossings at small internuclear distances, and we assume that the the electronic couplings are zero outside this region. This implies that the diabatic quantum defects can be joined smoothly with the adiabatic quantum defects computed from our *ab initio* potentials outside the interaction region.

In Fig. 6 the lowest $^1\Sigma_g^+$ resonant state potential energy and autoionization width are displayed in comparison to previously published results by Tennyson [44] and Sanchez and Martin [45]. The present resonant energy is slightly lower than Refs. [44,45]. The total autoionization width is slightly larger at some points of internuclear distance but agree in the general shape. The same procedure has been applied to determine the potential and autoionization width of the lowest resonant state in the $^1\Sigma_u^+$, $^1\Pi_g$, and $^1\Pi_u$ symmetries. A good overall agreement with [44,45] is found for these symmetries. The molecular data are available as Supplemental Material [39].

III. THEORY AND MODEL

A. Inclusion of rotational couplings

The theoretical model that we use for MN is largely the same as in previous studies and has been described in detail elsewhere; see, e.g., Ref. [22]. Here we will outline how the rotational couplings are included in our model. We use the following conventions for describing the coordinates of the system. In a *space-fixed* coordinate system, the position of the electrons are described by the coordinates (x_i, y_i, z_i), and the nuclear coordinates are given by (R, θ, ϕ). We perform a transformation to a coordinate system which moves with the molecule, i.e., a *body-fixed* coordinate system, since this transforms the rotational couplings to potential form. For the electrons, we will let the coordinates (ξ_i, η_i, ζ_i) denote the new coordinates in the body-fixed coordinate system. We take the body-fixed coordinate system to be such that the ζ axis coincides with the internuclear distance vector $\vec{R}$ and lies in the xy plane. The η axis is orthogonal to the $z\zeta$ plane. This is the same convention as in, e.g., [46]. The Hamiltonian H is transformed to a body-fixed coordinate system. The total wave function is expanded in a complete set of simultaneous eigenstates of H, $\vec{J}^2$, and J_z and is written as a rotation of a

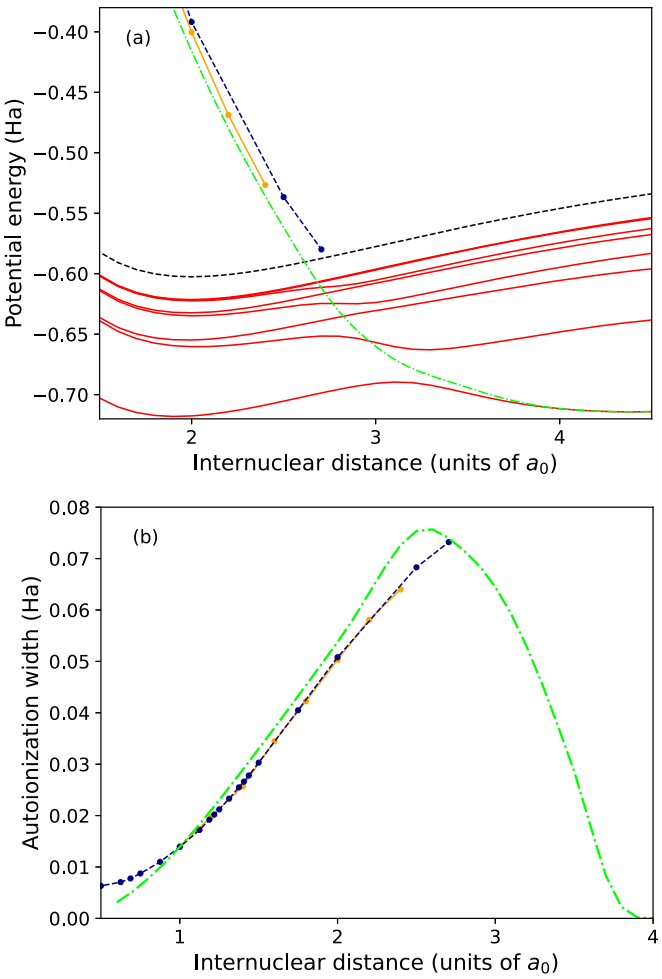

FIG. 6. (a) Energy and (b) total autoionization width of the lowest $^1\Sigma_g^+$ resonant state. The green dash-dotted line shows the present calculation while the solid orange and dashed dark blue lines show the results of Ref. [44] and Ref. [45], respectively.

body-fixed wave function. We further expand the wave function in terms of a complete set of orthonormal eigenfunctions of the L_ζ operator and write down the body-fixed coupled radial Schrödinger equation in an adiabatic representation. We let $F_{n'J\Lambda}$ denote the radial part of the nuclear wave function. The quantum number Λ is the projection of the electronic orbital angular momentum onto the molecular axis, and it can be both positive and negative when $|\Lambda| > 0$. By taking into account parity and inversion symmetry, one can connect states of Λ to those of $-\Lambda$ and thus eliminate this arbitrariness. We also introduce symmetry-adapted electronic wave functions, denoted by $\Phi_{n\Lambda}$, which are eigenfunctions of the reflection operator σ_η. Using these conventions, the radial Schrödinger equation for the nuclear states takes the form [46,47]

$$\left[-\frac{1}{2\mu}\frac{\partial^2}{\partial R^2}\mathbf{I}+\frac{J(J+1)-\Lambda^2}{2\mu R^2}\mathbf{I}-E\mathbf{I}\right]\mathbf{F}_{J\Lambda}$$
$$=-\mathbf{V}^\Lambda\mathbf{F}_{J\Lambda}+\frac{1}{2\mu}\left[2\mathbf{f}^\Lambda\frac{\partial}{\partial R}+\mathbf{D}^\Lambda\right]\mathbf{F}_{J\Lambda}$$
$$-\frac{1}{2\mu R^2}\mathbf{B}^\Lambda\mathbf{F}_{J\Lambda}-\frac{1}{\mu R^2}C^-\mathbf{\Pi}^{\Lambda,\Lambda-1}\mathbf{F}_{J\Lambda-1}$$
$$+\frac{1}{\mu R^2}C^+\mathbf{\Pi}^{\Lambda,\Lambda+1}\mathbf{F}_{J\Lambda+1}, \tag{7}$$

where

$$V_{ij}^\Lambda=\langle\Phi_{i\Lambda}|H_{el}|\Phi_{j\Lambda}\rangle\,\delta_{ij},$$
$$f_{ij}^\Lambda=\langle\Phi_{i\Lambda}|\frac{\partial}{\partial R}|\Phi_{j\Lambda}\rangle\,,$$
$$D_{ij}^\Lambda=\langle\Phi_{i\Lambda}|\frac{\partial^2}{\partial R^2}|\Phi_{j\Lambda}\rangle\,,$$
$$B_{ij}^\Lambda=\langle\Phi_{i\Lambda}|(L_\xi^2+L_\eta^2)|\Phi_{j\Lambda}\rangle\,,$$
$$C^\pm=\sqrt{J(J+1)-\Lambda(\Lambda\pm1)},$$
$$\Pi_{ij}^{\Lambda,\Lambda\pm1}=\langle\Phi_{i\Lambda}|iL_\eta|\Phi_{j\Lambda\pm1}\rangle\,. \tag{8}$$

In Eq. (7), Λ runs only over nonnegative integers, and the term containing $\mathbf{F}_{J\Lambda-1}$ is not present if $\Lambda-1<0$.

For diatomic molecules it is possible to perform a strict diabatization, where an orthogonal transformation of the states transforms the nonadiabatic couplings among a finite number of coupled states to potential form [22,48]. For Eq. (7), the procedure needs to be generalized slightly because we now include states of different symmetries that are coupled by rotational couplings. We suppose that, for each symmetry Λ, the adiabatic to diabatic orthogonal transformation matrix is given by [48]

$$\left(I\frac{\partial}{\partial R}+\mathbf{f}^\Lambda\right)\mathbf{T}_\Lambda=0. \tag{9}$$

The diabatic radial wave functions are given by the transformation

$$\widetilde{\mathbf{F}}_{J\Lambda}=\mathbf{T}_\Lambda^{\mathrm{T}}\mathbf{F}_{J\Lambda}. \tag{10}$$

Note that the transformation matrix $\mathbf{T}_\Lambda^{\mathrm{T}}$ for different symmetries will have different dimensions depending on how many states we include in that symmetry. By inserting the transformation (10) into the matrix Schrödinger equation and multiplying from the left by $\mathbf{T}_\Lambda^{\mathrm{T}}$, we obtain

$$\left[-\frac{1}{2\mu}\frac{\partial^2}{\partial R^2}\mathbf{I}+\frac{J(J+1)-\Lambda^2}{2\mu R^2}\mathbf{I}-E\mathbf{I}\right]\widetilde{\mathbf{F}}_{J\Lambda}$$
$$=-\widetilde{\mathbf{V}}^\Lambda\widetilde{\mathbf{F}}_{J\Lambda}-\frac{1}{2\mu R^2}\widetilde{\mathbf{B}}^\Lambda\widetilde{\mathbf{F}}_{J\Lambda}-\frac{1}{\mu R^2}C^-\widetilde{\mathbf{\Pi}}^{\Lambda,\Lambda-1}\widetilde{\mathbf{F}}_{J\Lambda-1}$$
$$+\frac{1}{\mu R^2}C^+\widetilde{\mathbf{\Pi}}^{\Lambda,\Lambda+1}\widetilde{\mathbf{F}}_{J\Lambda+1}, \tag{11}$$

where

$$\widetilde{\mathbf{V}}^\Lambda=\mathbf{T}_\Lambda^{\mathrm{T}}\mathbf{V}^\Lambda\mathbf{T}_\Lambda, \tag{12}$$
$$\widetilde{\mathbf{\Pi}}^{\Lambda,\Lambda-1}=\mathbf{T}_\Lambda^{\mathrm{T}}\mathbf{\Pi}^{\Lambda,\Lambda-1}\mathbf{T}_{\Lambda-1}. \tag{13}$$

Equation (11) is solved separately for the gerade and ungerade manifolds.

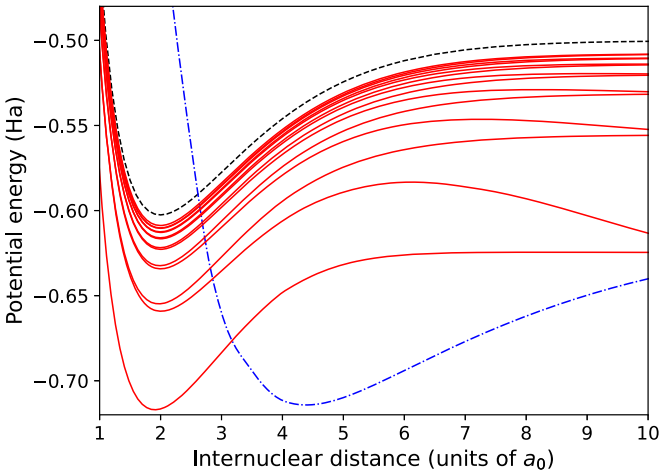

FIG. 7. Quasidiabatic potential curves of $^1\Sigma_g^+$ symmetry. Rydberg states are shown as red solid curves, the H_2^+ potential by the dashed black curve, and the resonant state by the blue dash-dotted curve.

B. The quasidiabatic model

A quasidiabatic model is introduced in order to include electronic resonant states (and thereby to incorporate autoionization) and to include couplings between the resonant states and the Rydberg manifolds. The quasidiabatic model is known to accurately describe the molecular system at small internuclear distances and for higher excited electronic states. The eigenvalues of the quasidiabatic potential matrix are approximately equal to the computed Born-Oppenheimer adiabatic energies at small internuclear distances. Thus, once the quasidiabatic potential matrix is set up and its eigenvalues are obtained, we can combine these with our *ab initio* potential curves. In this way we can include an arbitrary number of higher excited states in order to assess their influence on the MN cross section.

At small internuclear distances, the adiabatic potential curves are part of Rydberg series converging to the ground state of the H_2^+ ion plus a free electron with orbital angular momentum quantum number l. The Rydberg state potential curves are given by the well known Rydberg formula

$$V_i(R) = V_{\rm ion}(R) - \frac{1}{2\left[\nu_i^d(R)\right]^2}, \tag{14}$$

where $\nu_i^d(R)$ is the diabatic effective quantum number. The effective quantum number is given by $\nu_i^d(R) = n_i - \mu_l(R)$ where n_i is the principal quantum number and where $\mu_l(R)$ is the quantum defect. In the quasidiabatic picture, we let the resonant state cross the potential of the ion and then proceed to cross the diabatic Rydberg states. This is illustrated in Fig. 7 for $^1\Sigma_g^+$ symmetry.

In the present model we let the resonant state couple to all the Rydberg states included in the model, but we assume the Rydberg states do not couple to each other. To put this in mathematical terms, we introduce the electronic (quasidiabatic) resonant state, $|\phi_r^{qd}\rangle$, along with the diabatic Rydberg states, $|\phi_i^{qd}\rangle$, and these states are defined by the following conditions [49]:

$$\langle\phi_r^{qd}|\phi_i^{qd}\rangle = 0, \tag{15}$$

$$\langle\phi_i^{qd}|\phi_j^{qd}\rangle = \delta_{ij}, \tag{16}$$

$$\langle\phi_r^{qd}|H_{el}|\phi_r^{qd}\rangle = V_r^{qd}(R), \tag{17}$$

$$\langle\phi_i^{qd}|H_{el}|\phi_j^{qd}\rangle = V_{ij}^{qd}(R)\delta_{ij}, \tag{18}$$

$$\langle\phi_r^{qd}|H_{el}|\phi_i^{qd}\rangle = V_{ri}^{qd}(R) = V_{ir}^{qd}(R), \tag{19}$$

where the electronic coupling between the resonant and Rydberg states are obtained using the scaling relation [50]:

$$V_{ri}^{qd}(R) = \sqrt{\frac{\Gamma_l(R)}{2\pi}}\left[\nu_i^d(R)\right]^{-3/2}. \tag{20}$$

With these definitions, the bound part of the electronic Hamiltonian in a given symmetry has the following matrix representation:

$$H_{el} = \begin{pmatrix} V_r^{qd} & V_{r1}^{qd} & V_{r2}^{qd} & \dots & V_{rn}^{qd} \\ V_{1r}^{qd} & V_{11}^{qd} & 0 & \dots & 0 \\ V_{2r}^{qd} & 0 & V_{22}^{qd} & \dots & 0 \\ \vdots & \vdots & \vdots & \ddots & 0 \\ V_{nr}^{qd} & 0 & 0 & \dots & V_{nn}^{qd} \end{pmatrix}. \tag{21}$$

By diagonalizing this matrix we obtain an approximation of the adiabatic potential curves at small internuclear distances. The matrix in Eq. (21) is real, and symmetric and hence it can be diagonalized by

$$\mathbf{V}^{\rm ad} = \mathbf{S}^{\rm T}\mathbf{V}^{qd}\mathbf{S}. \tag{22}$$

We can also obtain approximative nonadiabatic coupling elements from the transformation matrix $\mathbf{S}$ by noting that Eq. (22) implies that

$$\phi_i^{\rm ad} = \sum_k (S^{\rm T})_{ik}\phi_k^{qd}, \tag{23}$$

and hence that

$$f_{ij}^{\rm ad}(R) = \langle\phi_i^{\rm ad}|\frac{d}{dR}|\phi_j^{\rm ad}\rangle = \sum_k (S^{\rm T})_{ik}\frac{d}{dR}S_{kj} + \sum_{kl}(S^{\rm T})_{ik}\langle\phi_k^{qd}|\frac{d}{dR}|\phi_l^{qd}\rangle S_{lj}. \tag{24}$$

The second term requires that we compute $\langle\phi_k^{qd}|\frac{d}{dR}|\phi_l^{qd}\rangle$, which can be approximated by the scaling relations introduced in [51]. This term is small and we therefore neglect it.

Once we have transformed the quasidiabatic potentials to the adiabatic representation and computed the approximative nonadiabatic couplings we can combine the potentials with the calculated *ab initio* adiabatic potentials. We can then use, for instance, the lowest M *ab initio* potentials in a given symmetry. For the radial couplings among these states we use the *ab initio* data. For higher excited states, $i > M$, we then use the approximative potentials that we have obtained

by transforming the quasidiabatic potentials to the adiabatic representation. The radial couplings among these states and between the *ab initio* calculated potentials and the approximative potentials are obtained using Eq. (24). We can then use the new combined *ab initio* and approximated adiabatic potentials and nonadiabatic couplings to transform to the strict diabatic representation as described above.

To conclude the discussion of the quasidiabatic model, one should also note that we need to consider the coupling between the resonant state and the continuum. The electronic Hamiltonian of (21) is the bound part of the full electronic Hamiltonian

$$H_{el}^{\text{full}} = \begin{pmatrix} \epsilon\delta(\vec{\epsilon}-\vec{\epsilon}') & V_{\epsilon r}^{qd} & 0 & 0 & \dots & 0 \\ V_{r\epsilon}^{qd} & V_{r}^{qd} & V_{r1}^{qd} & V_{r2}^{qd} & \dots & V_{rn}^{qd} \\ 0 & V_{1r}^{qd} & V_{11}^{qd} & 0 & \dots & 0 \\ 0 & V_{2r}^{qd} & 0 & V_{22}^{qd} & \dots & 0 \\ \vdots & \vdots & \vdots & \vdots & \ddots & \vdots \\ 0 & V_{nr}^{qd} & 0 & 0 & \dots & V_{nn}^{qd} \end{pmatrix}, \tag{25}$$

where we let ϵ denote the energy of the continuum. The quantity $V_{\epsilon r}^{qd}$ is the coupling between the resonant state and the continuum. By using the PQ formalism of Feshbach [52,53] and assuming a local approximation [54–57] it is possible to show that these couplings lead to a Schrödinger equation of nuclear motion in a complex potential:

$$\begin{aligned} &\left[-\frac{1}{2\mu}\frac{\partial^2}{\partial R^2}\mathbf{I} + \frac{J(J+1)-\Lambda^2}{2\mu R^2}\mathbf{I} - E\mathbf{I}\right]\widetilde{\mathbf{F}}_{J\Lambda} \\ &\quad = -\widetilde{\mathbf{V}}^{\Lambda}\widetilde{\mathbf{F}}_{J\Lambda} + \frac{i}{2}\widetilde{\mathbf{W}}^{\Lambda}\widetilde{\mathbf{F}}_{J\Lambda} - \frac{1}{2\mu R^2}\widetilde{\mathbf{B}}^{\Lambda}\widetilde{\mathbf{F}}_{J\Lambda} \\ &\qquad - \frac{1}{\mu R^2}C^{-}\widetilde{\mathbf{\Pi}}^{\Lambda,\Lambda-1}\widetilde{\mathbf{F}}_{J\Lambda-1} + \frac{1}{\mu R^2}C^{+}\widetilde{\mathbf{\Pi}}^{\Lambda,\Lambda+1}\widetilde{\mathbf{F}}_{J\Lambda+1}, \end{aligned} \tag{26}$$

where the imaginary part of the potential matrix, $\widetilde{\mathbf{W}}^{\Lambda}$, is given by

$$\widetilde{\mathbf{W}}^{\Lambda} = \mathbf{T}^{T}\mathbf{W}^{\Lambda,\text{ad}}\mathbf{T} = \mathbf{T}^{T}\mathbf{S}^{T}\mathbf{W}^{\Lambda,qd}\mathbf{S}\mathbf{T}. \tag{27}$$

The matrix $\mathbf{W}^{\Lambda,qd}$ is the imaginary part of the potential matrix in the quasidiabatic representation and has only one nonzero element, given by $\Gamma(R)$, at the same index as the resonant state. Because we now have a complex potential, the Hamiltonian will be non-Hermitian at small internuclear distances where the imaginary part of the potential is nonzero. The equations are solved for the nuclear wave functions using positive real values of the total energy. The scattering theory can therefore be formulated in the usual way, and the fact that the Hamiltonian is non-Hermitian at small internuclear distances introduces no further difficulties.

The local approximation requires the assumption that the vibrational channels of the ion that are open at each collision energy form a complete set. For $H^+ + H^-$ MN, this is true only for high collision energies, and thus the local approximation is strictly not valid for low collision energies. However, at low energies the cross section to $n = 3$ is completely dominating owing to the strong nonadiabatic radial couplings at 36 a_0 [22], and hence it is not likely that the small internuclear distances where autoionization takes place are reached.

C. Differential cross section

Scattering of $H^+ + H^-$ involves identical nuclei and formulas for the MN differential cross section that takes this into account can be formulated by forming a linear combination of the direct and exchange scattering amplitudes. The direct and exchange scattering amplitudes are given by [58,59]

$$f_{ij}^{d}(E,\theta) = \tfrac{1}{2}\left[f_{ij}^{g}(E,\theta) + f_{ij}^{u}(E,\theta)\right], \tag{28}$$

$$f_{ij}^{ex}(E,\theta) = \tfrac{1}{2}\left[f_{ij}^{g}(E,\theta) - f_{ij}^{u}(E,\theta)\right], \tag{29}$$

where the superscripts g and u refer to gerade and ungerade symmetry, respectively. The scattering amplitude is given by [42]

$$f_{ij}(\theta,E) = \sum_{J}(2J+1)e^{i(\sigma_i^J+\sigma_j^J)}f_{ij}^{J}(E)P_J(\cos\theta), \tag{30}$$

where

$$f_{ij}^{J}(E) = \frac{S_{ij}^{J}(E)-\delta_{ij}}{2i\sqrt{k_i k_j}}. \tag{31}$$

The phase factor $e^{i(\sigma_i^J+\sigma_j^J)}$ is present because we have one Coulomb channel in the symmetries $^1\Sigma_g^+$ and $^1\Sigma_u^+$, respectively. The Coulomb phase is given by $\sigma_i^J = \arg\Gamma(J+1+i\eta_i)$ where the Sommerfeld parameter, $\eta_i = \mu q_1 q_2/k_i$, is set to zero for non-Coulomb channels.

Because the nuclei are identical, there is no way of differentiating between the direct and exchange interactions. Furthermore, the potential asymptotically correlating with the ion-pair state may be of either $^1\Sigma_g^+$ or $^1\Sigma_u^+$ symmetry, and therefore the reflection symmetry of the electronic wave functions needs to be considered. Taking these things into account, the differential cross section is given by [42,58,59]

$$\begin{aligned} \frac{d\sigma_{ij}}{d\Omega}(E,\theta) &= \frac{3}{4}\frac{k_i}{k_j}\left|f_{ij}^{g,\text{odd}}(E,\theta) + f_{ij}^{u,\text{even}}(E,\theta)\right|^2 \\ &\quad + \frac{1}{4}\frac{k_i}{k_j}\left|f_{ij}^{g,\text{even}}(E,\theta) + f_{ij}^{u,\text{odd}}(E,\theta)\right|^2, \end{aligned} \tag{32}$$

where the superscripts even and odd indicate that the summation of the scattering amplitudes are over even and odd angular momentum quantum numbers, respectively.

IV. RESULTS AND DISCUSSION

A. Mutual neutralization total cross section

The $H^+ + H^-$ MN cross section has been calculated for energies between 0.001 and 600 eV. In Fig. 8 the calculated cross section, including covalent states that correlate with the $n \leqslant 4$ limits, autoionization and rotational couplings, is shown in comparison to previous theoretical calculations [16,19,21,22] and experimental measurements [17,20]. The present result is in reasonable agreement with the experimental data by Szucs *et al.* [17] and Peart *et al.* [20] for energies below about 200 eV. The measured cross section of Ref. [20] does not exhibit the E^{-1} behavior for low energies predicted by Wigner's

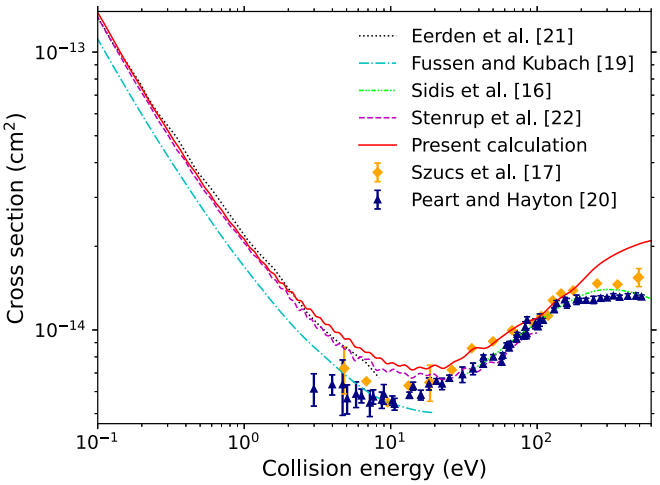

FIG. 8. Calculated total $H^+ + H^-$ MN cross section, including autoionization and rotational couplings, in comparison to previous theoretical calculations [16,19,21,22] and experimental measurements [17,20].

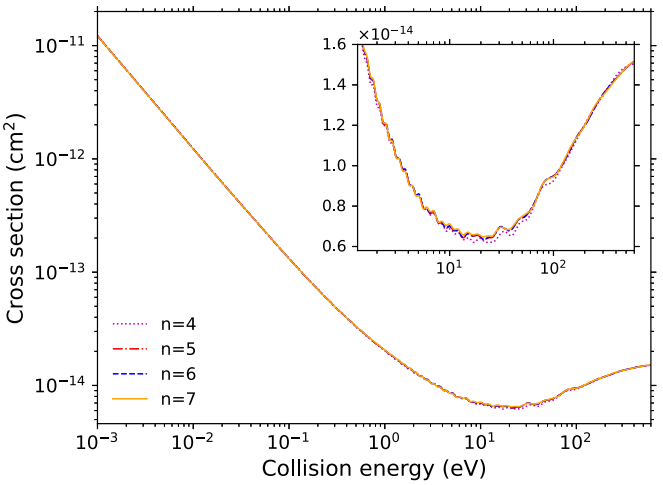

FIG. 10. Calculated total $H^+ + H^-$ MN cross section with the inclusion of higher excited states. The label $n = 4$ indicates that excited states were included that correlate to limits up to and including the $n = 4$ limit and so on.

threshold law [60] and which is seen in the theoretical results. The present calculation agrees with the low-energy Landau-Zener calculation by Eerden *et al.* [21] and is a factor of about 1.2 larger than that of Fussen and Kubach [19]. Compared to the previous calculation of Stenrup *et al.* [22], which included states up to the $n = 3$ limit and did not include autoionization or rotational couplings, the present calculation is larger for energies above a few eV while the two calculations overlap for smaller energies.

The effects of including autoionization and rotational couplings in the model have been investigated and the results are presented in Fig. 9. When rotational couplings are included, the cross section is increased by about 10% between 5 and 20 eV. At higher energies, the increase ranges between 15% and 20%. The magnitude of the cross section is increased because rotational couplings will induce interactions with more covalent states. The effect of autoionization has been assessed by turning the imaginary part of the potential matrix on and off in the calculations. When autoionization is included, the cross section is slightly decreased, which can be understood since there is a loss of flux to the ionization continuum. This effect is small, however. The present calculation only included the lowest resonant state in each symmetry considered in the model, and in principle higher lying resonant states also could contribute as a loss mechanism. Additionally, autoionization from Rydberg states due to nonadiabatic interactions is not included in present model. This could explain why our calculated cross section in Fig. 8 is larger than the experimental cross sections at high collision energies. In principle, rotational couplings to $^1\Delta_{g/u}$ states could also be included, which would be a second-order effect. An additional calculation was made where we included these couplings using a pure precession approximation [61]. This increased the cross section by at most 1.6% and made an equally small change in the branching ratios.

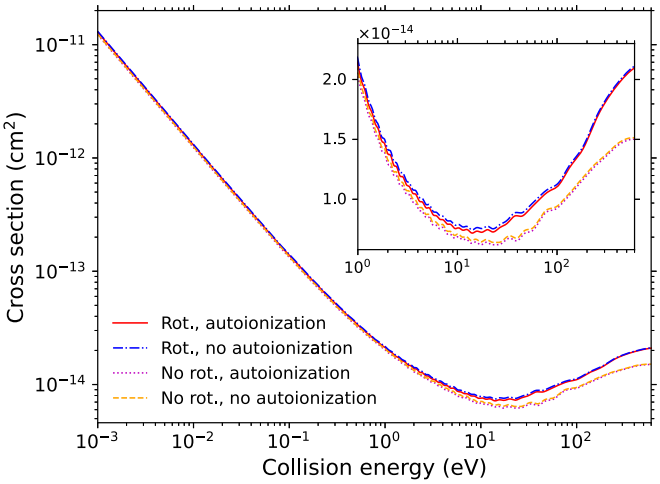

FIG. 9. Calculated total $H^+ + H^-$ MN cross section with and without rotational couplings and autoionization.

In order to assess the effect of higher excited states, the total MN cross section has been calculated including covalent states that asymptotically correlate with the limits $n = 4$, $n = 5$, $n = 6$, and $n = 7$. These calculations have been carried out using the quasidiabatic model described in Sec. III B (without rotational couplings) and the results are shown in Fig. 10. The cross sections almost entirely overlap in the energy range considered and thus the influence of higher excited states is negligible. Excited states that asymptotically correlate with limits $n > 4$ have significant radial nonadiabatic couplings only at small internuclear distances and therefore they have a small contribution to the magnitude of the total MN cross section.

B. Final state distributions

From the cross section calculations we are also able to obtain information on the final state distributions. Figure 11 shows the calculated $n = 2$, $n = 3$, and $n = 4$ branching ratios of the MN process, calculated with and without autoionization and rotational couplings. The $n = 1$ branching ratio is negligible in all cases and is not shown in Fig. 11. As a

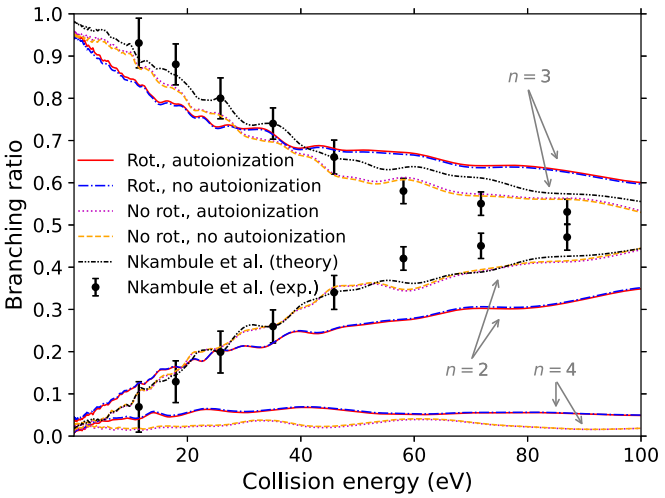

FIG. 11. Branching ratios of $H^+ + H^-$ MN. Also shown are the calculated and measured results of Ref. [23].

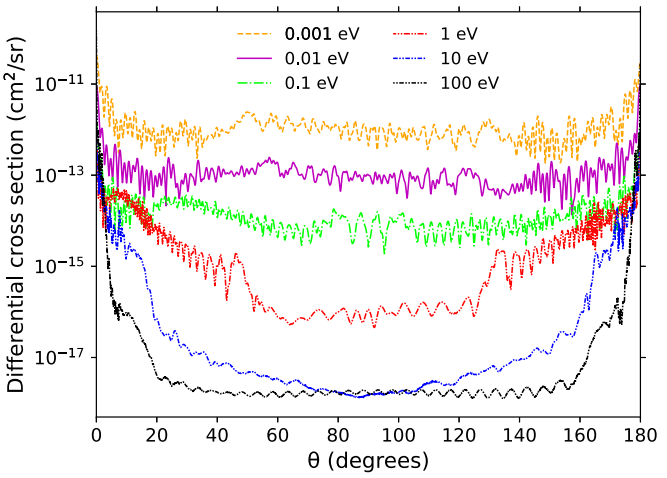

FIG. 12. Differential cross section of MN in $H^+ + H^-$ collisions at selected energies.

comparison, the black dotted lines and the black dots show the results of a previous combined experimental and theoretical study [23]. In the previous theoretical study, covalent states that correlate with the limits $n = 1, 2, 3$ were included and no rotational couplings nor autoionization were considered. The calculated and measured branching ratios were found to be in good agreement for energies below 50 eV. It was suggested that higher excited states, rotational couplings and autoionization are possible explanations of the disagreement at high energies. From Fig. 11 we can conclude that with the inclusion of the $n = 4$ states there is a redistribution from the $n = 3$ channels to the $n = 4$ channels making the $n = 3$ branching ratio smaller. The agreement of the $n = 3$ branching ratio with experiment is somewhat better than [23] for energies larger than about 50 eV. Autoionization has a negligible effect on the branching ratios. The inclusion of rotational couplings has a large influence on the $n = 2$ and $n = 3$ branching ratios. However, the agreement with experiment when rotational couplings are included is worse than the previous theoretical prediction of Ref. [23]. Measuring the $n = 4$ channel is experimentally challenging because the $n = 4$ fragments are not well separated from the $n = 3$ fragments. However, even if we assume that the $n = 4$ fragments can not be resolved, the agreement with the experiment at high collision energies is worse than the calculation of Ref. [23]. The branching ratios to states of $n > 4$ are at the most of order of 10^{-2} and are thus negligible.

For the H_2 system, some of the nonadiabatic couplings are nonzero asymptotically. This could induce transitions between states at arbitrarily large internuclear distances. This problem arises because the coordinates used to describe the collision complex are not suited to describe the free atoms [62]. A similar problem arises in semiclassical theory where the remedy is the inclusion of electron translation factors [63,64]. In our calculations, such a solution is not practical. One approach to this problem is the reprojection method [62,65,66], which in principle could be applied in the present case. However, the nonadiabatic couplings that are nonzero asymptotically are only among covalent states and their asymptotic values are small compared to their values at the avoided crossings. In order to assess the influence that these nonadiabatic couplings have on our results, we have performed calculations at various energies where we integrated the log derivative to 80 a_0 instead of 50 a_0. This was found to have a negligible influence on the cross section and branching ratios for the entire range of energies considered here.

C. Differential cross section

The differential cross section of MN in $H^+ + H^-$ collisions has been calculated at selected energies and the result is presented in Fig. 12. In these calculations both autoionization and rotational couplings are included. The cross section is dominated by forward and backward scattering and is symmetric at all energies. As the energy is increased, the cross section becomes more symmetric. In the forward and backward directions, the cross sections exhibit fast oscillations. In the forward direction, the angle at which these oscillations change character decreases as the energy increases. The reverse is true in the backward direction. The differential cross section of $H^+ + H^-$ MN has previously been calculated by Nkambule *et al.* [23]. Their calculation did not include the phase factor containing the Coulomb phase (see Sec. III C) and is therefore incorrect. This phase factor is not present in the expression for the total cross section but must be included when computing the differential cross section if there is a Coulomb channel present. Interestingly, the reason that the previously calculated differential cross section [23] is not symmetric around $\theta = 90^\circ$ is not due to the missing Coulomb phase. Using the same set of potentials and couplings, we do not obtain symmetric differential cross sections. However, with our new potentials and couplings, we obtain a symmetric differential cross section even if we in the calculation only include the same number of states (all $n \leqslant 3$ covalent states) as in the previous study.

The shape of the differential cross section is altered as the energy increases from 0.1 eV to 1 eV. In order to understand this pattern, the direct and exchange differential cross sections have been calculated. A comparison of the direct and exchange differential cross sections to the total differential cross section is shown in Fig. 13. The direct differential cross

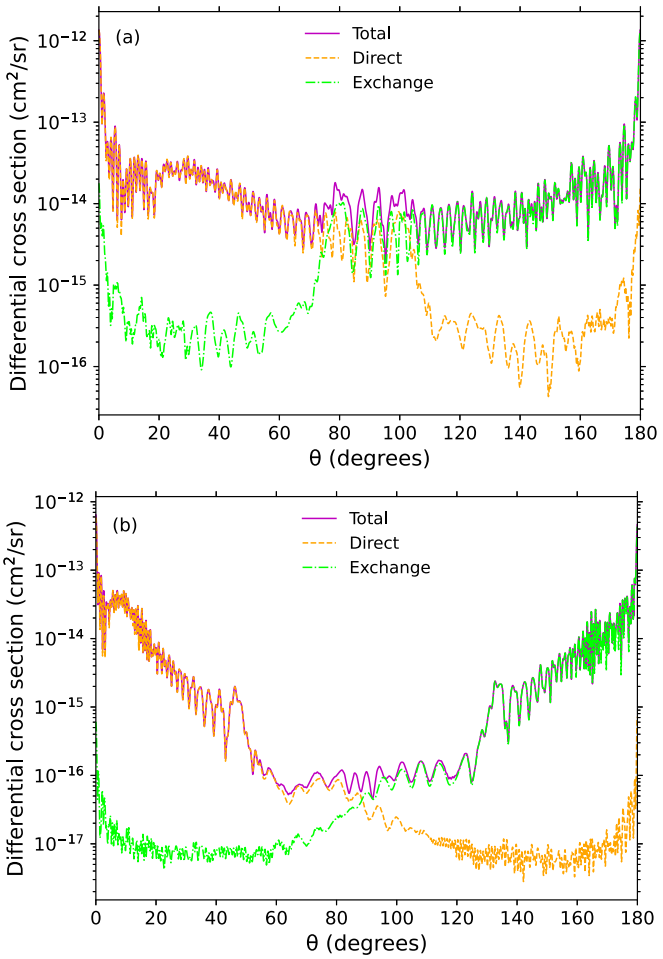

FIG. 13. Comparison of the direct and exchange differential cross sections at (a) $E = 0.1$ eV and (b) $E = 1.0$ eV.

section is dominated by forward scattering while the exchange differential cross section is dominated by backwards scattering. This gives rise to the symmetric total differential cross section. Comparing the direct differential cross section at the two energies 0.1 eV and 1.0 eV, we see that the angle where the oscillations change character decreases as the energy increases. The reverse is true for the exchange differential cross section. For larger collision energies, as is seen in Fig. 13(b), this gives rise to the dip in the total differential cross section. This dip is not present at lower energies because of the overlap of the direct and exchange differential cross sections.

In order to investigate how rotational couplings and autoionization influence the differential cross section, calculations have been performed with and without these effects. The result is shown in Fig. 14 for a collision energy of 1.0 eV. The differential cross sections differ negligibly for angles in the intervals 20° to 50° and 130° to 160°. The main difference is for angles between 50° and 130° where the cross sections including autoionization is somewhat smaller.

V. SUMMARY

We have studied mutual neutralization in collisions of $H^+ + H^-$ and we have investigated the role of autoionization,

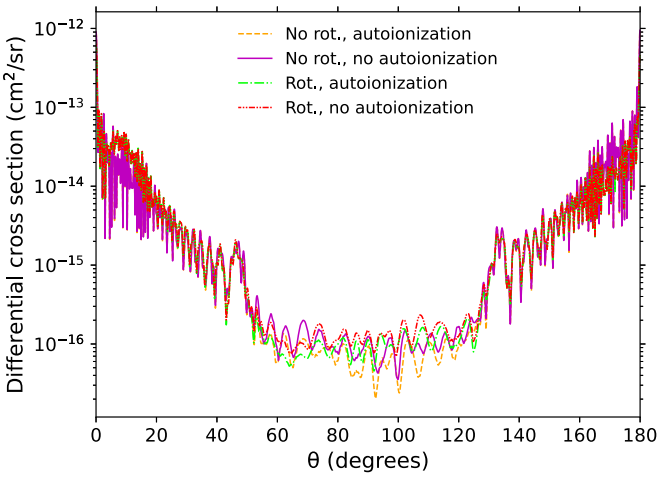

FIG. 14. Differential cross section of MN in $H^+ + H^-$ collisions at $E = 1.0$ eV calculated with and without rotational couplings and autoionization.

rotational couplings and excited covalent states associated with $n \geqslant 4$. Relevant adiabatic potential curves of $^1\Sigma_g^+$, $^1\Sigma_u^+$, $^1\Pi_g$, and $^1\Pi_u$ symmetries as well as radial and rotational nonadiabatic couplings have been computed *ab initio*. It was found that rotational couplings cause a significant increase of the total cross section at collision energies above a few eV. Autoionization plays the role of a loss mechanism but the influence on the total cross section is small. Applying a quasidiabatic model, the importance of higher excited states ($n \geqslant 4$) has been investigated. These states have a negligible influence on the total cross section. The branching ratios of the $H^+ + H^-$ MN process have been computed with and without the effects of rotational couplings and autoionization. When rotational couplings are included, the agreement with experiment becomes worse over almost the entire energy range considered here. The differential cross section of $H^+ + H^-$ MN has been calculated at selected energies. The differential cross sections are symmetric with respect to the scattering angle and are dominated by forward and backward scattering.

The model of H_2 can be applied to study other processes such as double charge transfer, associative ionization, dissociative recombination and resonant ion-pair formation. We have here presented a method that makes it possible to include an accurate description of bound electronic states as well as Rydberg states and electronic resonant states. We include couplings between bound states at both small and large internuclear distances as well as couplings to the ionization continuum. The model can be applied to other diatomic systems for which it is possible to carry out accurate structure calculations.

ACKNOWLEDGMENTS

We acknowledge M. Sahlin for performing the quantum chemical calculations. This work was performed as a part of the project "Probing charge- and mass-transfer reactions on the atomic level," supported by the Knut and Alice Wallenberg Foundation (2018.0028).

[1] G. Eklund, J. Grumer, S. Rosén, M. C. Ji, N. Punnakayathil, A. Källberg, A. Simonsson, R. D. Thomas, M. H. Stockett, P. Reinhed *et al.*, Phys. Rev. A **102**, 012823 (2020).

[2] G. Eklund, J. Grumer, P. S. Barklem, S. Rosén, M. C. Ji, A. Simonsson, R. D. Thomas, H. Cederquist, H. Zettergren, and H. T. Schmidt, Phys. Rev. A **103**, 032814 (2021).

[3] J. Grumer, G. Eklund, A. M. Amarsi, P. S. Barklem, S. Rosén, M. C. Ji, A. Simonsson, H. Cederquist, H. Zettergren, and H. T. Schmidt, Phys. Rev. Lett. **128**, 033401 (2022).

[4] N. de Ruette, A. Dochain, T. Launoy, R. F. Nascimento, M. Kaminska, M. H. Stockett *et al.*, Phys. Rev. Lett. **121**, 083401 (2018).

[5] R. D. Rundel, K. L. Aitken, and M. F. A. Harrison, J. Phys. B: At. Mol. Phys. **2**, L954 (1969).

[6] T. D. Gaily and M. F. A. Harrison, J. Phys. B: At. Mol. Phys. **3**, L25 (1970).

[7] J. Moseley, W. Aberth, and J. R. Peterson, Phys. Rev. Lett. **24**, 435 (1970).

[8] B. Peart, R. Grey, and K. T. Dolder, J. Phys. B: At. Mol. Phys. **9**, L369 (1976).

[9] D. R. Bates and J. T. Lewis, Proc. Phys. Soc. A **68**, 173 (1955).

[10] R. E. Olson, J. R. Peterson, and J. T. Moseley, J. Chem. Phys. **53**, 3391 (1970).

[11] R. K. Janev and A. R. Tancic, J. Phys. B: At. Mol. Phys. **5**, L250 (1972).

[12] K. Roy and S. C. Mukherjee, Phys. Rev. A **7**, 130 (1973).

[13] F. Borondo, A. Macias, and A. Riera, Phys. Rev. Lett. **46**, 420 (1981).

[14] F. Borondo, A. Macias, and A. Riera, Chem. Phys. **81**, 303 (1983).

[15] F. Borondo, A. Macias, and A. Riera, Chem. Phys. Lett. **100**, 63 (1983).

[16] V. Sidis, C. Kubach, and D. Fussen, Phys. Rev. A **27**, 2431 (1983).

[17] S. Szucs, M. Karemera, M. Terao, and F. Brouillard, J. Phys. B: At. Mol. Phys. **17**, 1613 (1984).

[18] B. Peart, M. A. Bennett, and K. Dolder, J. Phys. B: At. Mol. Phys. **18**, L439 (1985).

[19] D. Fussen and C. Kubach, J. Phys. B: At. Mol. Phys. **19**, L31 (1986).

[20] B. Peart and D. A. Hayton, J. Phys. B: At. Mol. Opt. Phys. **25**, 5109 (1992).

[21] M. J. J. Eerden, M. C. M. van de Sanden, D. K. Otorbaev, and D. C. Schram, Phys. Rev. A **51**, 3362 (1995).

[22] M. Stenrup, A. Larson, and N. Elander, Phys. Rev. A **79**, 012713 (2009).

[23] S. M. Nkambule, N. Elander, A. Larson, J. Lecointre, and X. Urbain, Phys. Rev. A **93**, 032701 (2016).

[24] J. N. Bardsley, Recombination processes in atomic and molecular physics, in *Atomic and Molecular Collision Theory*, edited by F. A. Gianturco (Springer, Boston, 1980), pp. 123–164

[25] L. Wolniewicz and K. Dressler, J. Chem. Phys. **100**, 444 (1994).

[26] G. Staszewska and L. Wolniewicz, J. Mol. Spectrosc. **212**, 208 (2002).

[27] K. Aidas, C. Angeli, K. L. Bak, V. Bakken, R. Bast, L. Boman, O. Christiansen, R. Cimiraglia, S. Coriani, P. Dahle *et al.*, WIREs Comput. Mol. Sci. **4**, 269 (2014).

[28] Dalton, a molecular electronic structure program, Release v2016.2, http://daltonprogram.org (2019).

[29] T. H. Dunning, J. Chem. Phys. **90**, 1007 (1989).

[30] L. Wolniewicz, J. Mol. Spectrosc. **169**, 329 (1995).

[31] L. Wolniewicz and G. Staszewska, J. Mol. Spectrosc. **220**, 45 (2003).

[32] G. Corongiu and E. Clementi, J. Chem. Phys. **131**, 034301 (2009).

[33] G. Corongiu and E. Clementi, J. Phys. Chem. A **113**, 14791 (2009).

[34] H. Nakashima and H. Nakatsuji, J. Chem. Phys. **149**, 244116 (2018).

[35] Y. I. Kurokawa, H. Nakashima, and H. Nakatsuji, Phys. Chem. Chem. Phys. **21**, 6327 (2019).

[36] C. Galloy and J. C. Lorquet, J. Chem. Phys. **67**, 4672 (1977).

[37] L. Wolniewicz, T. Orlikowski, and G. Staszewska, J. Mol. Spectrosc. **238**, 118 (2006).

[38] K. Dressler and L. Wolniewicz, Can. J. Phys. **62**, 1706 (1984).

[39] See Supplemental Material at http://link.aps.org/supplemental/10.1103/PhysRevA.106.062821 for data on adiabatic potential curves, radial and rotational nonadiabatic coupling elements, resonant state energies, electronic couplings, quantum defects, and the hydrogen basis set.

[40] T. N. Rescigno, C. W. McCurdy, A. E. Orel, and B. H. Lengsfield III, *The Complex Kohn Variational Method in Computational Methods for Electron-Molecule Scattering*, edited by W. H. Huo and F. A. Gianturco (Plenum, New York, 1995).

[41] A. U. Hazi, Phys. Rev. A **19**, 920 (1979).

[42] J. R. Taylor, *Scattering Theory: The Quantum Theory of Nonrelativistic Collisions* (Wiley, New York, 1972).

[43] A. Corana, M. Marchesi, C. Martini, and S. Ridella, ACM Trans. Math. Softw. **13**, 262 (1987).

[44] J. Tennyson, At. Data Nucl. Data Tables **64**, 253 (1996).

[45] I. Sanchez and F. Martin, J. Chem. Phys. **106**, 7720 (1997).

[46] J. Grosser, Z. Phys. D: At. Mol. Clusters **3**, 39 (1986).

[47] A. Macías and A. Riera, Phys. Rep. **90**, 299 (1982).

[48] C. A. Mead and D. G. Truhlar, J. Chem. Phys. **77**, 6090 (1982).

[49] T. F. O'Malley, Phys. Rev. **162**, 98 (1967).

[50] J. Weiner, F. Masnou-Seeuws, and A. Giusti-Suzor, Adv. At. Mol. Opt. Phys. **26**, 209 (1990).

[51] A. V. Stolyarov, V. I. Pupyshevy, and M. S. Child, J. Phys. B **30**, 3077 (1997).

[52] H. Feshbach, Ann. Phys. **5**, 357 (1958).

[53] H. Feshbach, Ann. Phys. **19**, 287 (1962).

[54] A. Herzenberg, J. Phys. B **1**, 548 (1968).

[55] D. T. Birtwistle and A. Herzenberg, J. Phys. B **4**, 53 (1971).

[56] L. Dube and A. Herzenberg, Phys. Rev. A **11**, 1314 (1975).

[57] L. Dube and A. Herzenberg, Phys. Rev. A **20**, 194 (1979).

[58] F. Masnou-Seeuws and A. Salin, J. Phys. B: At. Mol. Phys. **2**, 1274 (1969).

[59] R. M. Jordan and P. E. Siska, J. Chem. Phys. **69**, 4634 (1978).

[60] E. P. Wigner, Phys. Rev. **73**, 1002 (1948).

[61] H. Lefebvre-Brion and R. W. Field, *Perturbations in the Spectra of Diatomic Molecules* (Academic Press, Orlando, FL, 1986).

[62] J. Grosser, T. Menzel, and A. K. Belyaev, Phys. Rev. A **59**, 1309 (1999).

[63] D. R. Bates and R. McCarroll, Proc. R. Soc. London A **245**, 175 (1958).

[64] J. B. Delos, Rev. Mod. Phys. **53**, 287 (1981).

[65] A. K. Belyaev, D. Egorova, J. Grosser, and T. Menzel, Phys. Rev. A **64**, 052701 (2001).

[66] A. K. Belyaev, Phys. Rev. A **82**, 060701(R) (2010).